International Journal of Multiphase Flow 36 (2010) 184–192

Contents lists available at ScienceDirect

International Journal of Multiphase Flow

journal homepage: www.elsevier.com/locate/ijmulflow

Reconstruction of film thickness time traces for wavy turbulent free falling films

M. Kostoglou, K. Samaras, T.D. Karapantsios *

Division of Chemical Technology, Department of Chemistry, Aristotle University of Thessaloniki, University Box 116, 541 24 Thessaloniki, Greece

ARTICLE INFO

Article history:
Received 24 July 2009
Received in revised form 27 October 2009
Accepted 6 November 2009
Available online 10 November 2009

Keywords:
Falling film
Reconstruction
Surface morphology
Statistical analysis

ABSTRACT

The direct simulation of the hydrodynamics of falling films is a computationally difficult task. Especially in the case of wavy turbulent films the required effort is beyond the current computational capabilities. An alternative approach is to reduce the complexity of the problem using experimental information. In this spirit the present work focuses on the reconstruction of film thickness traces employing information acquired from experimental data. The reconstruction procedure for large waves is quite straightforward utilizing directly descriptive parameter distributions found from the analysis of experimental data. The rest of the film waves are reconstructed based on three criteria: their heights obey a "universal distribution", their frequency is selected to match the experimental film thickness frequency and the overall film thickness time trace obeys a Weibull distribution. The final reconstruction algorithm is tested for wavy turbulent films over a broad range of Reynolds numbers with satisfactory results. Apart from efficient the code is robust and fast.

1. Introduction

The study of free falling films using both theoretical and experimental means is an evergreen subject able to produce results of widespread utilization. Liquid falling films are encountered in common process equipment in which heat and mass transfer processes occur (Collier, 1972). For instance, food industry has a major interest on the optimized design and operation of direct contact falling film evaporators and condensers (Karapantsios and Karabelas, 1995). Another important application of free falling films is gas absorption towers whose performance is strongly influenced by the film characteristics and especially from its surface waves structure (Webb, 1994). This is mainly due to the strong mass/heat transfer enhancement induced by surface waves not only by increasing the gas/liquid interfacial area but chiefly by creating a transverse velocity profile in the falling film.

There is a large amount of experimental work on the subject but despite its significance experimental data can offer only limited information on the film flow field (Ambrosini et al., 2002; Adomeit and Renz, 2000). On the contrary, theoretical modeling can give (at least in principle) the complete spatial and temporal description of the flow field and the surface structure of the film. Unfortunately, modeling of falling film hydrodynamics is not a simple task and despite the many efforts the current ability to predict the falling film characteristics is limited (Alekseenko et al., 1985; Chang et al., 1996; Meza and Balakotaiah, 2008). For the case of laminar flow there are no fundamental difficulties for the modeling task; the governing equations can be easily written down. The only problem is the very high computational effort required due the chaotic nature of the flow and the large aspect ratio (length/thickness) which must be considered in order to follow the development of the film characteristics.

Several approximating strategies for the reduction of the computational effort can be found in literature. In older studies the complete set of equations is solved for a pre-specified wave geometry that is determined from experimental observations (Wasden and Dukler, 1989). An alternative approach is the reduction of the set of the governing equations to an evolution problem for the film interface which can be solved efficiently for arbitrary flow length. Approaches of this type are met under the names of long wave equation (Benney, 1966), first and second order boundary layer approximation (Yu et al., 1995) and h–q (Mudunuri and Balakotaiah, 2006) model. Their common feature is the omission of some terms in the complete set of equations, the assumption of the shape of the transverse velocity profile and the application of a weighted residual principle to construct the equations for the unknown coefficients of the assumed shape.

The recent increase in computer power allowed also the solution of the complete system of equations to simulate large aspect ratio domains using periodic boundary conditions (Malamataris et al., 2002) or following the development of waves (Malamataris and Balakotaiah, 2008). Nevertheless, even more computer power is needed to reach the region of fully developed waves. Also the ad-

* Corresponding author. Tel.: +30 2310 99 7772; fax: +30 2310 99 7759.
E-mail addresses: kostoglu@chem.auth.gr (M. Kostoglou), ksamaras@chem.auth.gr (K. Samaras), karapant@chem.auth.gr (T.D. Karapantsios).

0301-9322/$ - see front matter © 2009 Elsevier Ltd. All rights reserved.
doi:10.1016/j.ijmultiphaseflow.2009.11.005

vance of techniques in the spirit of Volume of Fluid (VOF) permits the direct simulation of the evolution of falling films – avoiding interface tracking – in two or even three dimensions using the complete Navier Stokes equation (Kunugi and Kino, 2005; Kunugi et al., 2005). For computational reasons this approach is restricted to Reynolds numbers less than 100.

No simulation efforts for the case of turbulent wavy flow film can be found in literature except one based on a pre-specified wave shape (Ye et al., 2002). In turbulent wavy films the direct simulation based on Navier Stokes is out of the question for computational reasons whereas the use of Reynolds Averaged Navier Stokes with some $k-\varepsilon$ model introduces a new factor of uncertainty.

In brief, the experimental approach suffers from limited capacity for detailed and accurate information whereas the theoretical approach needs more computing power. An idea to overcome the disadvantages of the two approaches is to combine them. A possible way to do it is by reconstruction of a long interface shape (not just of a single wave as in the old approach but of a large time-span where many waves occur) determined from experimental data and then solve the governing equations in this known geometry. Evidently, such efforts are most valuable for high Reynolds numbers where other theoretical approaches fail. Along this line of thinking and taking into account the stochastic nature of the film shape evolution (in the sense of deterministic chaos) Touglidis et al. (2004) proposed a procedure for the reconstruction of thickness versus time traces, $h(t)$, of wavy turbulent falling films. Traces were produced algorithmically to exhibit similar local wave features and integral statistical properties with the experimentally measured traces. Data were from a single measuring station located 2.5 m downstream from liquid entry where the flow was considered as fully developed. Yet, Touglidis et al. approach was successful only for Re < 5500.

In the present work a new reconstruction technique is proposed using data of film thickness from four measuring stations along the flow and for a much broader range of Reynolds numbers. The final scope of the general reconstruction approach is to be able to create dynamic film thickness shape $h(x, t)$ (x distance, t time) for a specific downstream region along the flow and for a given set of parameters. These parameters are the Reynolds number, the Kapitza or Weber number and the downstream location along the flow. In the present case all the experiments were performed using the same fluid in just one temperature $T = 20 \pm 0.2$°C at the same measurement locations along the flow so the only actual parameter is the Re number controlled through the flow rate. For a given Reynolds the other parameters are uniquely determined. The shape reconstruction can be achieved by considering the temporal data $h_1(t)$ at the first measurement location and proceeding along the flow exploring the correlations between the data $h_i(t)$ of consecutive measurement locations. In any case the first step in this procedure is the successful reconstruction of the trace in a single measurement location which is the focus of the present work. It is noted that a first order approximation of $h(x, t)$ around the measurement point i, can be found by simply transforming time into distance multiplying it by wave celerity. Nevertheless the final aim is to reconstruct $h(x, t)$ along the whole measurement region. Combining the known $h(x, t)$ with mathematical models for the flow field, the velocity profiles will be estimated with a computational effort much less than if $h(x, t)$ was unknown.

The structure of the present work is the following: First, available information on large waves and how they can be used for the reconstruction is described. Next, some intuitive approaches to generate secondary (smaller) waves are presented. Finally, the reconstruction procedure is described in detail and several indicative results are given and discussed.

2. Background

Details on the experimental setup and procedures for obtaining film thickness data are given elsewhere (Karapantsios and Karabelas, 1995). We repeat here only some information essential to understand the experimental system where we applied the present analysis. Film flows are realized inside a vertical 5 cm id tube with 2.5 m total length. Data are obtained at distances 1.73, 1.83, 1.90 and 2.00 m from the liquid entry in order to avoid end effects. The analysis performed in our previous work (Kostoglou et al., 2009) showed non-detectable differences of film properties among the measurement locations. This indicates that the flow evolution along the region of measurements is very small so it can be ignored. This does not necessary mean that fully developed flow has been reached since there is evidence in literature that distances larger than 3–4 m are required for full flow development (Ganchev and Kozlov, 1973). In case of non-fully developed flow field the extent of flow development can differ from one Reynolds to another suggesting the distance from the liquid entry as a third state parameter of the analyzed flow (the other two are Reynolds number and temperature).

Data cover the range $830 \leqslant \mathrm{Re} \leqslant 11000$ with $\mathrm{Re} = 4\,\Gamma/\mu$, where Γ is the mass flow rate over the wetted perimeter of the tube and μ the dynamic viscosity of the liquid. Experiments are conducted with filtered, deaerated tap water at $T = 20° \pm 0.2$°C. Measurements of film thickness versus time are taken by the well known parallel wire conductance technique on which this group has considerable experience (e.g., Karapantsios et al., 1989, 1995). Flush mounted plugs furnished with two parallel wires ($\sim$0.5 mm diameter, $\sim$2 cm length and $\sim$2 mm apart in the horizontal direction) protruding laterally into the falling film are employed for measurement. Although the parallel wire technique is intrusive it is preferable to optical techniques which are unable to give reliable signals at steep slopes of the interface (Helbig et al., 2009) as is the case for the large waves of wavy turbulent films. On the other hand, techniques involving flush mounted electrodes are not sensitive to height variations for such thick films (Chu and Dukler, 1974). It must be stressed, however, that for the present study it is irrelevant which technique is used to obtain film thickness data since the analysis can be applied to data from any technique.

Data are collected with a 400 Hz sampling frequency which was found adequate for capturing the features of such films. Tests with frequencies up to 16 kHz did not yield any new film features implying that it is rather the spatial resolution (distance between parallel wires) than the temporal resolution that dictates measuring sensitivity. Three records of 5 s each are acquired at every flow rate (Reynolds number) and for all plug locations to check for repeatability and further increase the confidence of the calculated statistics. The estimated overall error in film thickness measurements – including, calibration, measurement, digitization and data handling is always less than 7%.

It is generally accepted (e.g. Telles and Dukler, 1970; Chu and Dukler, 1974; Takahama and Kato, 1980; Karapantsios et al., 1989) that a falling film consists of four elements: (i) substrate, (ii) large waves (also termed roll waves) which are waves with amplitude higher than the average film thickness, h_{ave}, (iii) ripples which have amplitude lower than h_{ave} and are located between large waves and (iv) capillary waves which are very small waves of high frequency that can be found anywhere at the surface of the film apart from the highest parts of large waves. Inspection of pertinent literature reveals that, apart from their size and frequency, there is no other generally accepted physically-based criterion for distinguishing capillary waves from ripples. By convention, as capillary waves are characterized small

film thickness undulations with amplitude at least about an order of magnitude smaller than the minimum film thickness and with frequency at least about an order of magnitude higher than the frequency of ripples. These characteristics are respected in the present work.

The scope of this paper is to propose a method of stochastically reconstructing film thickness traces resembling as much as possible those measured experimentally. There can be several ways of reconstruction based on different principles (e.g. based on Fourier spectra of the time series). It is believed that the reconstruction principles proposed by Touglidis et al. (2004) for an hierarchical approach based on the height of individual waves offer distinct advantages. The reconstruction of each element is based on different criteria. The most important element of the reconstruction is the region of large waves.

3. Reconstruction of local temporal data

3.1. Available information on large waves

First, large waves are considered as they constitute the largest and fastest region of liquid. In Touglidis et al. (2004) waves are chosen progressively from the highest one to smaller ones until a nominal frequency estimated from Fourier spectra analysis is reached. In the present work "large" are considered all waves as long as their height exceeds the average trace thickness. The idea is to "filter" the experimental time series data retaining only the large waves. Then the shape information of each wave is reduced by approximating it with a certain mathematical function with unknown parameters. Finally, the probability density functions (PDF) of these parameters are derived.

The details of the data analysis of the acquired large waves is presented elsewhere (Kostoglou et al., 2009). Here we present only a summary to allow the reader appreciate the reconstruction procedure. Large waves are approximated by the function

$$h = a + b \cdot \exp\left[-\frac{\left(c \cdot \ln\frac{t+e}{c}\right)^2}{2w^2}\right] \tag{1}$$

Parameters b, w and c stand, respectively, for wave amplitude (mm), wave time–length (s) and time–distance of the peak from the beginning of the wave (s). In particular, w is not the actual wave time–length but a representative parameter which has the merit to be independent from the other two (b, c) having a well defined physical meaning. The actual wave time–length P (defined as the time span between the two points of the wave having height φb with φ being a small number) is related to w through the relation $P = c \cdot \left[e^{\left(\frac{w}{c}\sqrt{-2\ln\varphi}\right)} - e^{\left(-\frac{w}{c}\sqrt{-2\ln\varphi}\right)}\right]$. Parameters a and e do not have any physical meaning regarding the wave shape; they are auxiliary parameters used solely to achieve the best possible fitting by the particular function.

The essential fitting parameters b, c, w are registered only if the fitting quality exceeds a certain value. In this way a few irregular large waves are disregarded. Several researchers have fitted the shape of large waves with the log-normal (Takahama and Kato, 1980) or Gamma distribution (Telles and Dukler, 1970) but the proposed distribution has the advantage that its parameters are uncorrelated to each other and so they obey independent PDFs. This means that the three dimensional PDF of the parameters b,c,w can be written as a product of three one dimensional PDFs. The PDFs of b, c and w are computed for each Reynolds number and each measurement location. The main conclusions regarding these PDFs are (Kostoglou et al., 2009):

(1) There is no dependence at any level of significance on measurement location. This observation confirms that the flow can be considered in a quasi-stationary state along all the examined measurement locations.
(2) The PDF of parameter w is independent from Reynolds number. So a single (master) PDF is constructed for w using all the available data (nine Reynolds numbers and four measurement locations). This distribution – $P_w(w)$ is shown in histogram form in Fig. 1.
(3) The PDF of parameter c is bimodal and exhibits a small dependence on Reynolds number. The low value mode of the PDF decreases and the high value mode increases as Reynolds increases. For practical purposes, this slight dependence can be ignored and the PDF of c can be assumed independent from Reynolds number during the reconstruction procedure. The average PDF of c–$P_c(c)$-constructed from all available data is shown in histogram form in Fig. 2.
(4) The situation for the PDF of b is more complex because it depends strongly on Reynolds number (but not on downstream measuring location). For the reconstruction procedure, the problem is how to construct a PDF function $-P_b(\mathrm{Re})$ for an arbitrary Reynolds number from the experimentally known PDFs at different Reynolds numbers. The experimental PDFs are different enough from each other to permit any kind of direct interpolation as it would be the case for just slightly different distributions. To overcome this problem the experimental PDFs are fitted by the following Gamma distribution:

$$P_b(y) = \frac{1}{c_2^{c_1}\Gamma(c_1)} y^{c_1-1} e^{-y/c_2} \tag{2}$$

where c_1 and c_2 are fitting parameters and Γ is the well known Gamma function defined as $\Gamma(y) = \int_0^\infty z^{y-1}e^{-z}dz$.

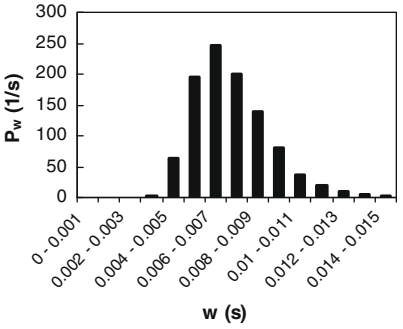

Fig. 1. Histogram of the experimental PDF for parameter w.

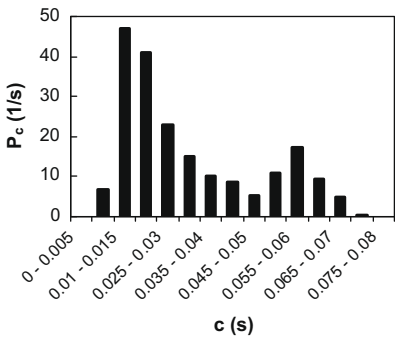

Fig. 2. Histogram of the experimental PDF for parameter c.

For all the experimental Reynolds numbers the fitting procedure has been very successful as it is shown for the typical comparison between experimental PDFs and fitting results in Fig. 3. The fitting parameters c_1 and c_2 are shown (with corresponding trendlines) versus Reynolds number in Fig. 4a and b. Both parameters increase with Reynolds number.

(5) Fig. 5 displays the experimental PDFs of the time intervals (Δt) between the peaks of consecutive large waves for three Reynolds number (representative of the whole studied Reynolds range). For the smaller Reynolds numbers the PDF is very close to the exponential shape indicating random deposition (placement) of large waves on the available time domain (no interaction between waves). This observation is in accordance with the random deposition wave procedure employed by Touglidis et al. (2004). For Reynolds number higher than 3000 a second mode emerges in the PDF and gradually grows as Reynolds increases. This behavior indicates a progressively increasing "repulsion" between large waves in the available time domain. This may explain the failure of the random deposition procedure of Touglidis et al. for Re > 5000. In order to account for a general PDF of Δt during the reconstruction, it is necessary to employ the technique of sequential addition of waves to the time series.

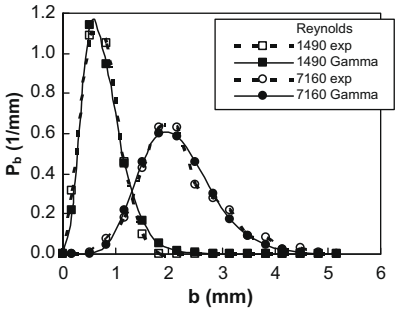

Fig. 3. Experimental PDF of parameter b and fitted Gamma distributions for two values of Reynolds number.

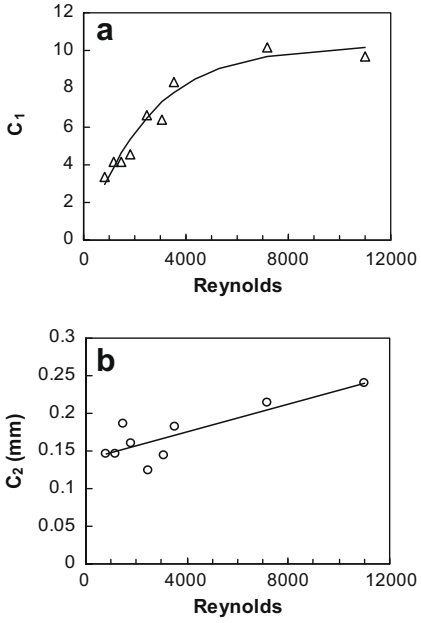

Fig. 4. Values of parameters $c1$ and $c2$ used to fit a Gamma distribution to experimental PDFs of b parameter versus Reynolds number.

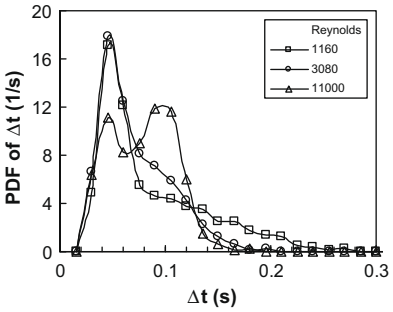

Fig. 5. Experimental PDFs of the interval Δt between the peaks of two consecutive large waves for three Reynolds numbers.

The PDFs of Δt for different Reynolds numbers span the same range of Δt so a PDF for an arbitrary Reynolds number can be constructed by linear interpolation between the experimental PDFs of the previous and following Reynolds number.

It is noted that although the analyzed data and the reconstruction procedure are strictly 2-D, several features presented above may be explained considering the 3-D structure of the waves. Waves on a free falling film are usually horseshoe-shaped, and the amplitude and shape of their sections along the flow vary significantly with transverse distance (Adomeit and Renz, 2000). Probability of accounting the central part of the wave by the measuring probe is comparable to probability of accounting one of the "tails" of the wave. e.g., the amplitude of the wave decreases from the central part to the "tails" so it influences the distribution of wave shape parameters. This fact may explain the bimodal shape of the PDF of parameter c in Fig. 2. This could be possible in case the transition from the steep front slope at the central part of the wave to the flat slope at the "tail" of the wave is rather sharp.

In addition, the presence of 3-D waves might explain the bimodal shape of some distributions of separation time in Fig. 5. The first peak in the distribution corresponds to nearly minimal possible distance between the two waves, traveling along the same line; the second peak corresponds to the nearly minimal possible distance between the two waves with different centerlines at the same actual minimal distance. The higher the number of waves per unit length (that grows with Re), the higher the possibility of two waves to be jammed to each other with different centerlines. Nevertheless, the above are just speculations. Only by having data at several transverse locations it is possible to reach an understanding of the 3-D structure of the waves and extend the present approach to the third dimension.

Other important statistical quantities of the film that are used in the reconstruction procedure is the average value h_{ave} of the film thickness, the standard deviation s_h and the minimum film thickness h_{min}. Computing these values for each experimental time trace, gives

$$h_{ave} = 1.78 \times 10^{-4}\mathrm{Re} + 0.22 \quad \mathrm{Re} \leqslant 3080$$
$$h_{ave} = 0.93 \times 10^{-4}\mathrm{Re} + 0.482 \quad \mathrm{Re} > 3080 \qquad (3)$$

Predictions of Eq. (3) deviate by less than 3% from the predictions of the empirical formula proposed by Karapantsios and Karabelas (1995) (their Eq. (2)) and is used here for simplicity.

The experimental s_h data cannot be fitted by a simple function since the scatter among runs is considerable, Fig. 6. The average h_{min} value (i.e., mean value among similar runs) can be represented versus Reynolds as

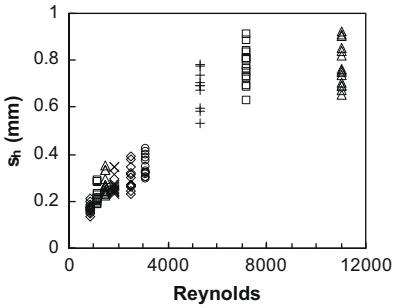

Fig. 6. Standard deviation of experimental film thickness time series versus Reynolds number.

$$\begin{aligned} h_{\min} &= 4\cdot 10^{-5}\mathrm{Re} + 0.129 \quad \mathrm{Re} \leqslant 2470 \\ h_{\min} &= 0.22 \quad 2470 < \mathrm{Re} \leqslant 7160 \\ h_{\min} &= 3\cdot 10^{-5}\mathrm{Re} + 0.0252 \quad \mathrm{Re} > 7160 \end{aligned} \tag{4}$$

The above representations for h_{ave} and h_{min} are by no means proposed as satisfactory descriptive formulas of their dependence on Re. It is simply a convenient way to incorporate them to the reconstruction procedure based on experimental evidence. In the future, more realistic models of general validity can be used.

In addition, it is noted that h_{min} does not show a consistent statistical behaviour. Only a very small portion of the time series (a few points per thousands) takes values less than $1.1 * h_{min}$ which means that h_{min} corresponds to a rare event and its value must be viewed with caution during the reconstruction procedure. Nevertheless h_{min} is a good choice for a parameter to use for the reconstruction of the substrate since the final reconstruction quality is very little sensitive to the exact value of h_{min}. In addition, it is very difficult to use other alternative statistical features of the substrate e.g. the average value, since they cannot be distinguished from ripples waves.

3.2. Approaches for the description of ripples and capillary waves

Since large waves influence both h_{ave} and s_h, their reconstruction must be an exact representation of the structure of experimental large waves as described by the criteria 1–5 above.

On the other hand, ripples are added in an empirical way in order to match the h_{ave} of the experimental time trace (since the influence of ripples on s_h is negligible). Therefore, the final distribution of ripple waves is not an actual representation of the actual data but expresses just a possibility. The selection of a particular model for ripples and its acceptance is based mainly on the comparison between reconstructed and experimental data.

Capillary waves are added empirically as a type of surface roughness without any relation to experimental data. This is so because the finite size of the measuring probe (distance between parallel wires), of the order of the size of capillary waves, did not allow resolving them accurately. One may argue that in such cases it is preferable to just smooth out roughness from experimental traces and forget about it. Yet, this was customary not done in literature in an effort to stress that capillary waves do exist on flowing films and in spite of measuring problems it is better not to ignore them giving the false impression that the surface is smooth. In line with this, we tried also to add empirically capillary waves on our wavy surfaces which apparently do not represent accurate data but emphasize that these films are not smooth and an algorithm should take care of their presence as well.

An important property of the experimental time series is that the distribution of the excess instantaneous film thickness $h(t) - h_{min}$ can be well described by a Weibull distribution (Karapantsios et al., 1989) (which is a generalized Gamma distribution in the context of statistics, a special type of the Pearson type III distribution in the context of polymer science and the Rosin–Ramler distribution in the context of particulate technology). The cumulative distribution of $y(t) = h(t) - h_{min}$ must be successfully fitted by the equation $1 - e^{-(y/\gamma)^k}$. As it is well known from the use of Rosin–Ramler distribution the problem of finding the parameters k and γ can be reduced after the proper data transformation to a straight line fitting problem. The requirement to represent the data by a Weibull distribution implies the existence of waves at the whole range of amplitudes. That is, the large waves alone can never fulfill this requirement. The good fitting of the cumulative distribution $h(t) - h_{min}$ by the Weibull function is a necessary requirement for the reconstructed data.

Regarding ripples, the key is to invoke an argument of shape similarity between different amplitude waves. That is, we assume that ripples have the same shape (i.e. Eq. (1)) as large waves and differ only in amplitude. On this account, the parameters c, w of ripples are assumed to follow the same PDF as the corresponding parameters of large waves. It is noted that there are always some waves slightly smaller than h_{ave} which are too large to be considered ripples. Also there are some waves slightly larger than h_{ave} disregarded during the fitting procedure and not counted as large waves. The above two types of waves were collectively termed as intermediate waves in Touglidis et al. (2004) and they were handled separately from ripples. This approach increased dramatically the computational load of Touglidis et al. (2004) procedure. Here an attempt is made to parameterize these waves simultaneously with ripples to reduce the complexity of the reconstruction algorithm. The main idea is that all other waves apart from large and capillary waves (henceforth referred to as "secondary waves") can be described by the w and c PDFs of large waves and by the following truncated Gamma distribution for b:

$$P_R(y) = \frac{y^{k_1-1}e^{-y/k_2}}{\int_0^{d(h_{ave}-h_{min})} z^{k_1-1}e^{-z/k_2}\,dz} \tag{5}$$

This distribution of secondary waves can be constructed according to the following criteria:

(i) The distribution is truncated to the wave amplitude $d(h_{ave} - h_{min})$. The particular scaling was chosen in order to minimize the influence of Reynolds number and to keep as parameter only the dimensionless quantity d. It is noted that $d = 1$ means that all secondary waves are below h_{ave} whereas for $d > 1$ there are secondary waves above h_{ave} (in the region of large waves).

(ii) The maximum value of the distribution, b_{Rmax}, corresponds to the most frequent amplitude of ripples. By simple algebra it can be found that $k_1 = 1 + b_{Rmax}/k_2$.

(iii) The value of the distribution at the point of truncation is parameterized by the cumulative value F of a non-truncated Gamma distribution at the truncation point $y = d(h_{ave} - h_{min})$. According to the above criteria the parameter k_2 can be found from the solution of the following equation:

$$\frac{1}{k_2^{1+b_{R\,max}/c_2}\,\Gamma(1 + b_{R\,max}/k_2)} \int_0^{d(h_{ave}-h_{min})} y^{b_{R\,max}/k_2} e^{-y/k_2}\,dy = F \tag{6}$$

The left hand side of this equation is transformed to an incomplete Gamma function which can be computed using special algorithms (Press et al., 1986). Then the equation is solved for k_2 using the bisection technique. Finally, k_1 and k_2 are substituted in Eq. (5) and the PDF of b of the secondary waves is derived.

4. Reconstruction procedure

The reconstruction procedure is as follows: First, a Reynolds number, a frequency (data points per second) and the time–

length of the reconstructed trace are introduced. At present, the frequency is set at 400 Hz (equal to the employed experimental sampling frequency) and the trace time–length is at 5 s, long enough for the stabilization of integral statistical quantities. The substrate thickness is set equal to the experimental value of h_{min} predicted by Eq. (4). The critical step in the reconstruction procedure is the generation and addition of large waves onto the substrate. The PDF of Δt between the peaks of waves are constructed by linear interpolation between the experimental PDF functions with Reynolds number as the interpolation parameter. The PDFs of w and c are fixed (not depended on Reynolds) and the PDF of b is given by the Gamma distribution with parameters taken by linear interpolating between the parameters values for the experimental PDFs shown in Fig. 4. An attempt to use fitted functions (e.g. trends lines in Fig. 4) instead of linear interpolation was not successful because the fitting value of k_2 is in some cases pretty different from the experimental values and the reconstructed trace properties are different from those of the experimental trace violating the major criterion of the success of reconstruction.

The PDFs of Δt, b, c, w are transformed to cumulative distributions. The uniformly distributed random numbers produced by the computer are transformed to random numbers from the above PDFs by employing the inversion approach. Having generated the parameters Δt, b, c, w of a new wave, this is added to the trace in such a way that its peak is located at position $t + \Delta t$ where t is the peak location of the previous wave. This procedure continues until covering the whole pre-specified time length. It must be noted that the number of large waves in the reconstructed trace is not an input parameter but a result produced by the algorithm. Furthermore, the employed procedure does not require repetitive corrections of the deposited waves in order to match the standard deviation of the experimental data as this quantity is automatically adjusted by proper handling of b and Δt distributions. These points are serious improvements compared to Touglidis et al. (2004).

After the addition of large waves the cumulative distribution of film thickness is calculated. Under no circumstances this distribution can be approximated by a Weibull distribution. In order to make this approximation possible not only ripples but also intermediate waves must be added. The proposed generalized distribution of secondary waves takes care of this.

The input parameters for the amplitude distribution of secondary waves are the frequency f_R, the most frequent amplitude b_{Rmax}, the fraction $F(0 < F < 1)$ and the length scaling parameter d. For a given set of these parameters, the PDF of b is constructed as described previously and values of the stochastic parameters b, c, w are produced using the inversion technique and the corresponding PDFs. The number of generated waves is computed according to the required frequency (see below). These waves are then deposited on the pre-specified time–length in a uniformly random way. A special deposition technique is employed during the deposition of secondary waves which takes care of possible overlapping between secondary and large waves such as at each point of the reconstructed series only points with the highest thickness value survive.

Regarding capillary waves, the aim is to produce the same surface roughness impression observed in the experimental traces. Due to their very small size certain assumptions can be made which ease the computations without a real effect on the statistical properties of the reconstructed time series. Capillary waves are initially assumed to have the specific wave shape described by Eq. (1). After extensive comparisons with experimental data their amplitude is chosen $b_{cap} = 0.025$ mm (roughly equal to $0.1 * h_{min}$) and time–length $P_{cap} = 0.005$ s. Capillary waves are added at a uniformly random fashion with a pre-selected high frequency (usually 1000 Hz). It must be stressed that this high frequency does not turn up from experimental evidence since the finite size of the measuring probe did not allow sensing accurately capillary waves. Instead, capillary waves parameters are chosen empirically based on a similarity concept with larger waves. The above parameters result in exceeding overlapping among capillary waves which practically means that their initial shape is lost and so the film surface appears to have a stochastic roughness. The deposition of capillary waves follows the same principle of survival of the highest points but they are allowed to have additive overlap only with the secondary waves and substrate but not with large waves. In addition to the reconstruction parameters f_R, b_{Rmax}, F, d, an increase of the substrate thickness h_{min} is permitted given the nature of this variable (discussed above).

Our attempt at this work is to achieve successful reconstructions for the Reynolds numbers of our experimental data by properly adjusting the above parameters. This attempt is proved successful for all Reynolds number:

(i) The average number of large waves is similar for the reconstructed and experimental results. This average number increase from 8.5 waves/s (Re = 830) to 13 waves/s (Re = 11000). The argument of independency of wave frequency from Reynolds (Touglidis et al., 2004) does not hold. This is somewhat not so surprising since those authors worked in a much narrower range of Reynolds numbers.

(ii) The average film thickness and standard deviation of the reconstructed film trace are similar to the experimental values. It is noted that an exact coincidence is without meaning because although the average data for the reconstructed traces are exact (taken from a large number of runs) the experimental averages are just estimations due to the limited number of data.

(iii) The cumulative distribution of the reconstructed film thickness is successfully fitted by the cumulative function of the Weibull distribution.

(iv) The reconstructed traces look alike the experimental ones.

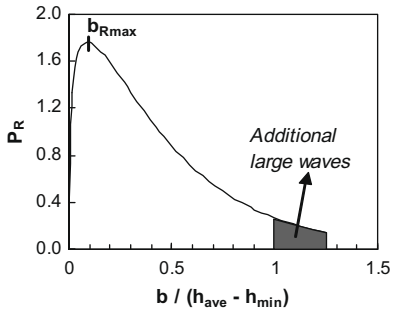

Fig. 7. Self-similar PDF of the amplitude b of secondary waves.

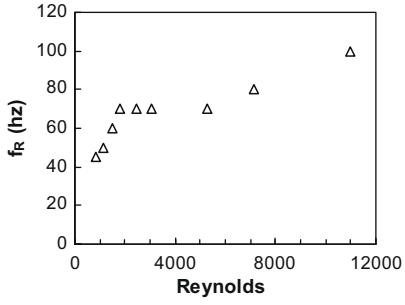

Fig. 8. Frequency of secondary waves needed for successful reconstruction of film thickness traces versus Reynolds number.

The issue is for what values of the unknown parameters (function of Reynolds in the general case) a successful reconstruction is achieved. The parameter b_{Rmax} is set equal to 0.1 (as for the uniform amplitude ripples in Touglidis et al., 2004). The parameter F is set equal to 0.95 corresponding to a small degree of truncation. Finally, the parameter d is set equal to 1.25 which means that a few large waves are also produced by the secondary wave algorithm. The PDF of b of secondary waves of course depends on Reynolds number (the larger the Reynolds the larger the b range) but the normalized variable $b/(h_{\mathrm{ave}} - h_{\mathrm{min}})$ absorbs all the Reynolds dependence and its PDF is independent from Reynolds. The shape of this PDF is shown in Fig. 7. So, the only remaining undefined parameter

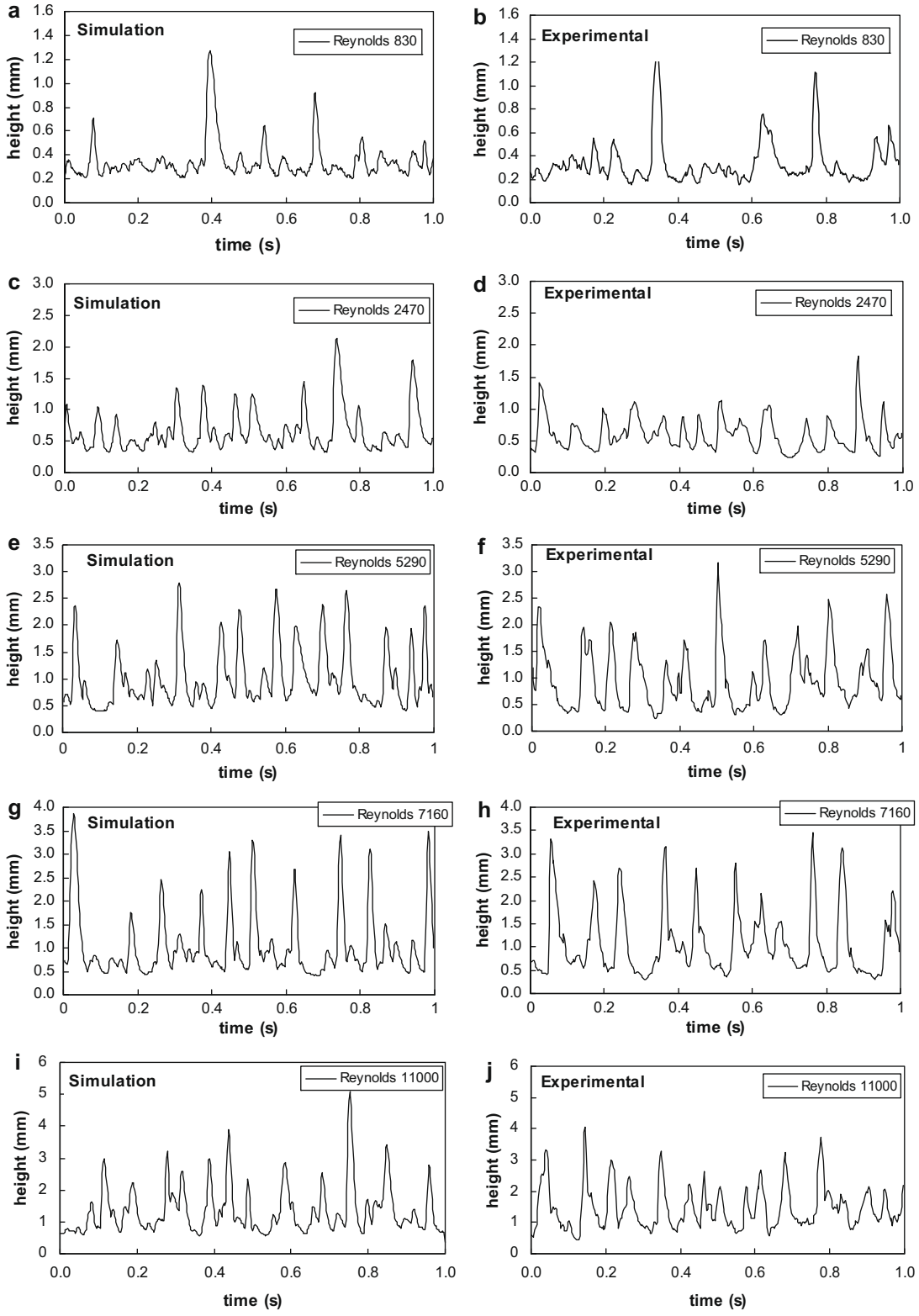

Fig. 9. Comparison between experimental and reconstructed film thickness data for five representative Reynolds numbers.

Table 1
Values of h_{ave} and s_h for the simulation cases presented in Fig. 9, juxtaposed with the corresponding Reynolds number experimental limits.

Reynolds	Fig. 9 case	Simulation values (mm)	Experimental limits (mm)
830	(a)	$h_{ave} = 0.346$	$0.33 < h_{ave} < 0.407$
		$s_h = 0.16$	$0.136 < s_h < 0.214$
2470	(c)	$h_{ave} = 0.657$	$0.593 < h_{ave} < 0.764$
		$s_h = 0.328$	$0.232 < s_h < 0.388$
5290	(e)	$h_{ave} = 1.022$	$0.825 < h_{ave} < 1.104$
		$s_h = 0.547$	$0.535 < s_h < 0.779$
7160	(g)	$h_{ave} = 1.15$	$1.065 < h_{ave} < 1.294$
		$s_h = 0.72$	$0.627 < s_h < 0.909$
11000	(i)	$h_{ave} = 1.444$	$1.39 < h_{ave} < 1.62$
		$s_h = 0.756$	$0.652 < s_h < 0.926$

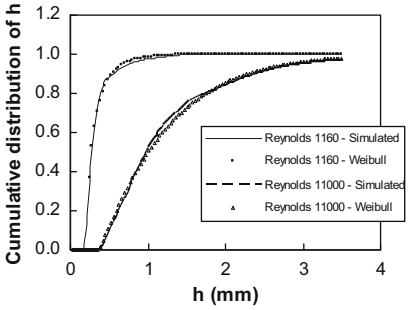

Fig. 10. Cumulative film thickness distribution and the corresponding fitting based on the Weibull distribution for two Reynolds numbers.

is the frequency of the secondary waves. Values of this parameter that are found to achieve successful reconstruction are shown versus Reynolds number in Fig. 8.

The shape of the frequency versus Re curve is very interesting. There is a linear dependence for $Re < 1800$, a constant value in the region $1800 < Re < 5500$ and again a linear dependence for $Re > 5500$. In order to get some idea about the origin of this behaviour let us start with the observation that the experimental frequency of ripples does not depend on Re number (Chu and Dukler, 1974). The frequency f_R, however, is not the observed frequency since many of these waves are lost due to overlapping by large waves or by other secondary waves. As Re increases the length of large waves increases (proportionally to b which depends on Re), the number of large waves increases and the length of the ripples increases (proportionally to b for ripples which depends on $h_{ave} - h_{min}$ which in turn depends on Re). To counterbalance these three factors, f_R must follow Fig. 8 in order to ensure a more or less Re independent reconstructed frequency of ripple waves.

5. Results and discussion

The reconstruction algorithm proved effective to reproduce film thickness traces of arbitrary duration and data frequency for any Reynolds number between 830 and 11000 by simply using a value of f_R taken from the linear interpolation between the data of Fig. 8. Some typical comparisons between the experimental and reconstructed traces for representative Reynolds number are presented in Fig. 9. The simulated traces match the experimental ones in the average film thickness value, standard deviation, wave frequency, wave separation (in time units) and in addition film they follow the Weibull distribution. Wave frequency and wave separation can be directly discerned and compared between simulations and experimental traces. This is not easy, though, for parameters such as the average film thickness and standard deviation. To support the correctness of the algorithm, Table 1 presents values of the average film thickness and standard deviation for the simulated traces of Fig. 9 and the experimentally determined range of these two parameters for the corresponding Reynolds number. Apart from the above match of statistical parameters, the reconstructed traces resemble the appearance of experimental traces – from a stochastic standpoint – for all the examined Reynolds numbers. It is worth mentioning that not only individual waves look alike but also double and triple waves are successfully reconstructed indicating that the dynamic nature of overriding/overlapping

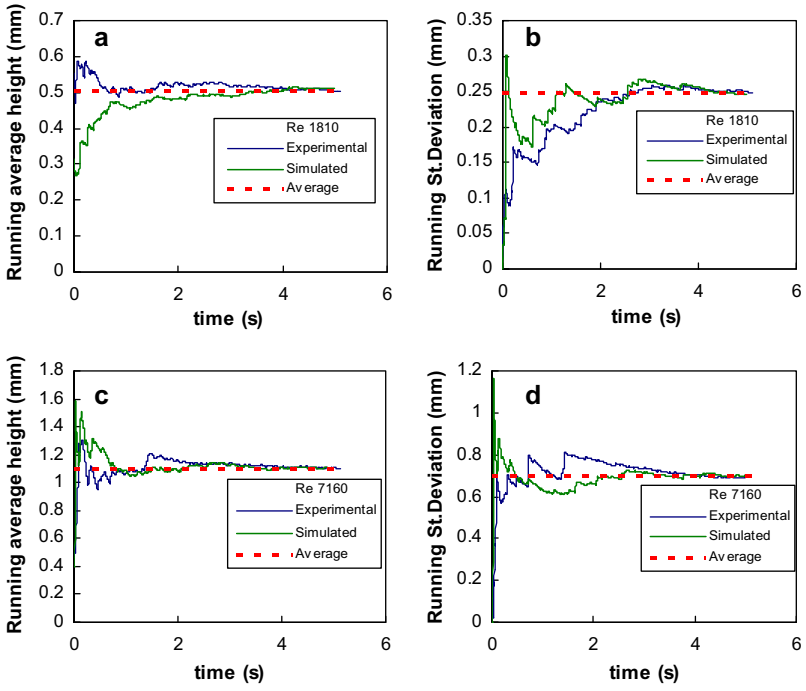

Fig. 11. Running values for the value average and standard deviation of film thickness versus time for two Reynolds numbers (experimental and reconstructed traces).

waves is efficiently depicted in the simulated data. This was indeed a challenge for Reynolds above 3000 where "repulsion" between large waves is noticed in the experimental traces and this is where the earlier work of Touglidis et al. (2004) has failed.

Fig. 10 compares the cumulative film thickness distributions of the reconstructed traces at two Reynolds numbers with the Weibull distribution. Evidently, the agreement is good over the full range of film thickness despite the considerably different shape of the cumulative distributions for the two Re numbers. This is a proof that the algorithm is equally effective regardless if there is a more uniform spread a wave sizes (high Re) or a dominant range of wave sizes (low Re).

From a technical point of view it is interesting to determine the minimum duration of the simulation which is required to achieve convergence in some integral properties such as the average value and the standard deviation of film thickness. Fig. 11 presents representative graphs (Re = 1810 and 7160) of these two statistical quantities against the duration of the film thickness trace. According to this figure, 4 s are enough for the satisfactory convergence of the two properties for both experimental and reconstructed data.

6. Conclusions

In the present work an algorithm is developed for the reconstruction of local film thickness time series for free falling films in turbulent wavy flow. The algorithm is based on information invoked from the behaviour of large waves in experimental data series. Large waves are reconstructed assuming a specific wave shape with size parameters directly sampled from PDFs derived using the experimental data. The rest of the waves are reconstructed based on certain assumptions and matching of unknown parameters in order to achieve reconstructed traces compatible with specific requirements. The parameters of the algorithm are determined for the case of water in the Reynolds number range between 830 and 11000 which is the range of existing experimental data. The developed algorithm is faster than real time and is capable to produce film thickness traces that cannot be distinguished from experimental ones over the examined range of Reynolds numbers.

Acknowledgment

Financial support by the European Space Agency through the project CBC (Convective Boiling and Condensation) (ESA-AO-2004-PCP-111/ELIPS-2) is gratefully acknowledged. This work is conducted under the umbrella of the COST P21 action: Physics of Droplets.

References

Adomeit, P., Renz, U., 2000. Hydrodynamics of three dimensional waves in laminar falling films. Int. J. Multiphase Flow 26, 1183–1208.
Alekseenko, S.V., Nakoryakov, V.Y., Pokusaev, B.G., 1985. Wave formation on vertical falling liquid film. AIChE J. 31, 1446–1460.
Ambrosini, W., Forgione, N., Oriolo, F., 2002. Statistical characteristics of a water film falling down a flat plate at different inclinations and temperatures. Int. J. Multiphase Flow 28, 1521–1540.
Benney, B.J., 1966. Long waves and liquid films. J. Math. Phys. 45, 150.
Chang, H.C., Demekhin, E.A., Kalaidin, E., 1996. Simulation of noise-driven wave dynamics on a falling film. AIChE J. 42, 1553–1568.
Chu, K.J., Dukler, A.E., 1974. Statistical characteristics of thin wavy films Part II. Studies of the substrate and the wave structure. AICHE J. 20, 695–706.
Collier, J.G., 1972. Convective Boiling and Condensation. McGraw-Hill, London.
Ganchev, B.G., Kozlov, V.M., 1973. Investigation of the gravitational flow of a liquid along the walls of a vertical channel of great length. J. Appl. Mech. Tech. Phys. 14 (1), 105–110.
Helbig, K., Nasarek, R., Gambaryan-Roisman, T., Stephan, P., 2009. Effect of longitudinal minigrooves on flow stability and wave characteristics of falling liquid films. J. Heat Transfer 131. 011601-1–011601-8.
Karapantsios, T.D., Karabelas, A.J., 1995. Longitudinal characteristics of wavy falling films. Int. J. Multiphase Flow 21, 119–127.
Karapantsios, T.D., Paras, S.V., Karabelas, A.J., 1989. Statistical characteristics of free falling films at high Reynolds numbers. Int. J. Multiphase Flow 15 (1), 1–21.
Karapantsios, T.D., Kostoglou, M., Karabelas, A.J., 1995. Local condensation rates of steam/air mixtures in direct contact with a falling liquid film. Int. J. Heat Mass Trans. 38 (5), 779–794.
Kostoglou, M., Samaras, K., Karapantsios, T.D., in press. Large wave characteristics and their downstream evolution at high Reynolds number falling films. AIChE J.
Kunugi, T., Kino, C., 2005. DNS of falling film structure and heat transfer via MARS method. Comput. Struct. 83, 455–462.
Kunugi, T., Kino, C., Serizawa, A., 2005. Surface wave structure and heat transfer of vertical liquid film flow with artificial oscillation. In: 5th International Symposium of Multiphase flow, Heat Mass Transfer and Energy Conversion.
Malamataris, N.A., Balakotaiah, V., 2008. Flow structure underneath the large amplitude waves of a vertically falling film. AICHE J. 54, 1725–1740.
Malamataris, N.A., Vlachogiannis, M., Bontozoglou, V., 2002. Solitary waves on inclined films: flow structure and binary interactions. Phys. Fluids 14, 1082–1094.
Meza, C.E., Balakotaiah, V., 2008. Modeling and experimental studies of large amplitude waves on vertically falling films. Chem. Eng. Sci. 63, 4704–4734.
Mudunuri, R.R., Balakotaiah, V., 2006. Solitary waves on thin falling films in the very law forcing frequency limit. AICHE J. 52, 3995–4003.
Press, W., Flannery, B., Teukolski, S., Vetterling, W., 1986. Numerical Recipes. Cambridge University Press, New York.
Takahama, H., Kato, S., 1980. Longitudinal flow characteristics of vertically falling liquid films without concurrent gas flow. Int. J. Multiphase Flow 6, 203–215.
Telles, A.S., Dukler, A.E., 1970. Statistical characteristics of thin, vertical, wavy, liquid films. Ind. Eng. Chem. Fund. 9, 412–421.
Touglidis, L.G., Karapantsios, T.D., Vlachos, N., Balouktsis, A.I., 2004. Surface morphology reconstruction of free falling films at high Reynolds numbers. Int. J. Multiphase Flow 30, 351–368.
Wasden, F.K., Dukler, A.E., 1989. Insights into the hydrodynamics of free falling wavy films. AICHE J. 35, 187–195.
Webb, R.L., 1994. Principles of Enhanced Heat Transfer. Wiley, London.
Ye, H., Yan, W., Jiang, Z., Li, C., 2002. Hydrodynamics of free-falling turbulent wavy films and implications for enhanced heat transfer. Heat Trans. Eng. 23, 48–60.
Yu, L.Q., Wasden, F.K., Dukler, A.E., Balakotaiah, V., 1995. Nonlinear evolution of waves on falling films at high Reynolds numbers. Phys. Fluids 7, 1886–1902.